Single-exposure 3D label-free microscopy based on color-multiplexed intensity diffraction tomography

Ning Zhou,[1,2,†] **Jiaji Li,**[1,2,†] **Jiasong Sun,**[1,2] **Runnan Zhang,**[1,2] **Zhidong Bai,**[1,2] **Shun Zhou,**[1,2] **Qian Chen,**[2,3] **and Chao Zuo**[1,2,*]

[1]*Smart Computational Imaging Laboratory (SCILab), School of Electronic and Optical Engineering, Nanjing University of Science and Technology, Nanjing, Jiangsu 210094, China*

[2]*Jiangsu Key Laboratory of Spectral Imaging & Intelligent Sense, Nanjing, Jiangsu 210094, China*

[3]chenqian@njust.edu.cn

*Corresponding author: zuochao@njust.edu.cn

†These authors contributed equally to this Letter

We present a 3D label-free refractive index (RI) imaging technique based on single-exposure intensity diffraction tomography (sIDT) using a color-multiplexed illumination scheme. In our method, the chromatic light-emitting diodes (LEDs) corresponding R/G/B channels in an annular programmable ring provide oblique illumination geometry that precisely matches the objective's numerical aperture. A color intensity image encoding the scattering field of the specimen from different directions is captured, and monochromatic intensity images concerning three color channels are separated and then used to recover the 3D RI distribution of the object following the process of IDT. In addition, the axial chromatic dispersion of focal lengths at different wavelengths introduced by the chromatic aberration of the objective lens and the spatial position misalignment of the ring LED source in the imaging system's transfer functions modeling are both corrected to significantly reduce the artifacts in the slice-based deconvolution procedure for the reconstruction of 3D RI distribution. Experimental results on MCF-7, Spirulina algae, and living *Caenorhabditis elegans* samples demonstrate the reliable performance of the sIDT method in label-free, high-throughput, and real-time (~24 fps) 3D volumetric biological imaging applications. © 2022 Optical Society of America

https://doi.org/10.1364/OL.442171

In the field of optical microscopy, three-dimensional (3D) imaging techniques play an increasingly important role in a variety of biomedical and life sciences applications, such as observing the morphology of living cells, fast dynamics in a large cell population, and tracking high-speed cell motions [1,2]. The refractive index (RI) distribution serves as a critical endogenous contrast agent, allows the determination of cellular structure and biophysical parameters with minimal sample manipulation, and the most widely used RI measurement technique is optical diffraction tomography (ODT). By introducing the principles of interferometry, the amplitude and phase information of an object can be simultaneously demodulated from the recorded interference patterns. Then, the 2D measurements of complex amplitude can further be synthesized together in the 3D spectrum domain with the Fourier diffraction theorem [3] by rotating the specimen or varying the illumination angles [4–6]. By recording a full set of angle-multiplexed projections in a single hologram, ODT can realize single-exposure 3D RI reconstruction [7,8]. Nevertheless, ODT needs to be implemented in well-controlled and customized optical setups coupled with coherent laser sources and mechanical angular scanning. Meanwhile, angle multiplexing has the problem of spectrum aliasing, which limits the effective numerical aperture (NA) of the imaging system.

Alternatively, 3D RI tomography can be realized by intensity-only measurements using axial scanning under symmetrical [9] or asymmetrical [10] illumination to obtain single or multiple intensity stacks. The volumetric RI distribution of the specimen is subsequently recovered through the deconvolution process between the captured intensity stacks and corresponding optical transfer function [11]. Nonetheless, the axial mechanical scanning may result in displacement errors and prolong the acquisition time, limiting the spatial and temporal resolution of 3D imaging. Similar approaches have been proposed to improve the temporal resolution of the intensity-based 3D RI tomography. Tian *et al.* presented a motion-free IDT technique using oblique light illumination and focal plane intensity-only image acquisition to recover 3D RI information [12]. The number of images required for IDT reconstruction was further decreased to eight images in our previous work [13], and experiments demonstrated that the imaging speed of living biological samples was up to 10.6 Hz. However, due to the limitation of camera frame rate and the low signal-to-noise ratio (SNR) caused by the reduction of exposure time, the existing imaging methods are difficult to achieve real-time (i.e., ≥24 fps) or higher frame rate 3D RI measurement.

In this work, we present a single-exposure IDT (sIDT), which addresses the above-mentioned limitations in conventional IDT by replacing the conventional LED illumination with an annular color-multiplexed source. Although the benefits of a color-multiplexed illumination scheme have been extensively studied in various fields of quantitative phase microscopy [14–16], its potential for spatial and temporal resolution improvement in

IDT imaging remains unexplored. By matching the illumination angle with the objective's numerical aperture precisely, the four-dimensional (4D) transfer functions (TFs) model of IDT [12,17] provide a broad Fourier coverage (approximately two times of the objective NA) with a few illumination angles and maximize the phase and absorption response both at low and high frequency. Nevertheless, the chromatic aberration of the objective lens would result in the focal plane misalignment of the three channels' quasi-monochromatic images separated from a color intensity image. Meanwhile, the R/G/B channels of annular LED illumination have different radius sizes due to the isolated distribution of luminous dyes of the three different color channels on each surface-mounted LED. Especially for high-NA imaging situations, any slight alignment variations in the experimental setup deviating from the expected illumination angles or focal plane positions will misalign the Fourier spectrum information [18]. Hence, the derived 4D TFs of the IDT model for single-wavelength illumination are not suitable for the imaging system with a color illumination scheme, and the incorrect TFs will inevitably cause significant reconstruction artifacts in the deconvolution process, thus degrading the final imaging resolution and axial reconstruction depth range.

To alleviate the axial misalignment issue of the focal plane induced by chromatic aberration, a cross correlation algorithm is implemented in our sIDT to determine the equivalent position of each color channel's focal plane under color-multiplexed illuminations. This approach starts by adjusting the LED position depending on the luminous dye of the green channel on the LED ring to precisely match the illumination angle with the objective's NA. Afterwards, the R/G/B channels of the LED ring are respectively employed as quasi-monochromatic illumination sources, and the complex 3D RI distribution of the specimen under various color illumination is reconstructed via the aIDT technology [13]. As illustrated in Fig. 1(a), the focal plane position of the complex RI distribution of diatom microalgae cells (S68786, Fisher Scientific) at the three color channels is inconsistent with each other. Then, the RI distribution image at the focus position of the green channel is treated as the datum focal plane image. Finally, calculating the cross correlation parameter Γ [19] between the complex 3D RI distribution matrix of red or blue channels and the datum focal plane image according to Eq. (1) yields the calibrated equivalent defocus distance for each color channel (i.e., Δf in Fig. 1):

$$\Gamma = \frac{\sum_m \sum_n Ir_{m,n} Is_{m,n}}{\sqrt{\left(\sum_m \sum_n Ir_{m,n}^2\right)\left(\sum_m \sum_n Is_{m,n}^2\right)}}, \qquad (1)$$

where I_r is the datum focal plane image of RI distribution under the green channel, I_s is the image of 3D RI distribution matrix under the red or blue illumination channels, and m and n are the two-dimensional coordinates of images. The large correlation index value indicates high relevance between I_r and I_s, as shown in Fig. 1(b). Then, the equivalent relative distance of the focal plane for each color channel is calibrated, and the chromatic-aberration compensated results of three channels can be obtained, as shown in Fig. 1(c). The aperture function $P'(\mathbf{u})$ with chromatic-aberration compensation can be expressed as

$$P(\mathbf{u})' = P(\mathbf{u}) \cdot \exp(ik_m \Delta f \sqrt{1 - \lambda^2(\mathbf{u})}), \qquad (2)$$

where $P(\mathbf{u})$ denotes the system's ideal pupil function (a low-pass filter with the cutoff frequency of $\frac{NA_{obj}}{\lambda}$), $k_m = k_0 n_m$ is the
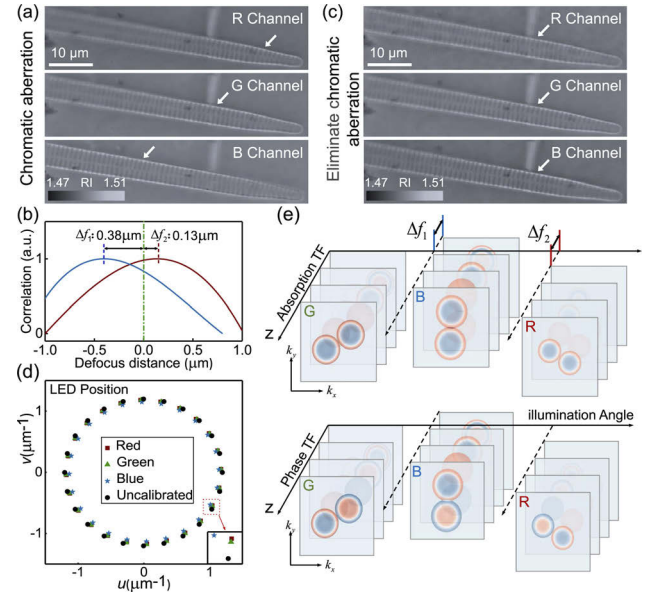
Fig. 1. Chromatic aberration and LED space position calibration of 4D TFs in sIDT theory. (a) Results of reconstructing the diatom cells on the focal plane using the images of the R/G/B channels, respectively. (b) Chromatic aberration parameters of objective lens matched by cross correlation algorithm. (c) Results of the reconstruction of diatom cells on the focal plane after the elimination of chromatic aberration. (d) LED position without (marked in black pattern) and with (marked in R/G/B pattern) the self-calibration method plotted in the spatial frequency coordinates. (e) Corrected 4D TFs.

wavenumber in medium, where $k_0 = 2\pi/\lambda$ indicates the wave vector in free space with λ being the illumination wavelength, and n_m is the RI of the surrounding medium. Here, Δf is the equivalent relative distance for the red and blue channel's focal plane, and $\mathbf{u}$ is the 2D spatial frequency variable.

Meanwhile, the lateral misalignment of the LED position degrades the quality of the 3D RI image, and the use of incorrect angles can lead to significant reconstruction artifacts. To solve this problem, our hardware employs a triaxial displacement platform to make the light source unit symmetrical with the optical axis center. Then we use a digital self-calibration program [20] proposed in our previous work to accurately correct the spatial position of each R/G/B light-emitting component in the LED ring [Fig. 1(d)]. After calibrating the LEDs' spatial position and the chromatic aberration parameters of the objective, the 4D TFs under color illumination can be derived through these calibrated parameters, as depicted in Fig. 1(e). The complex RI distribution of the specimen may then be recovered using a fast and effective slice-wise 3D deconvolution algorithm [13].

As depicted in Fig. 2(a), the sIDT experiments are performed based on a commercial inverted microscope (IX71, Olympus) equipped with a programmable LED ring (24 surface-mounted LEDs) and a color image sensor (PCO.edge 3.1, 2048 × 1536 resolution, 6.5 µm pixel pitch). The radius of the LED ring is ~39.3 mm, and this illumination unit is installed on the triaxial displacement platform to replace the existing illumination unit of the microscope. Three surface-mounted LEDs equally spaced on the LED ring use R/G/B luminous dyes (central wavelength 630/520/465 nm, respectively) and provide an oblique illumination geometry that precisely matches the numerical aperture
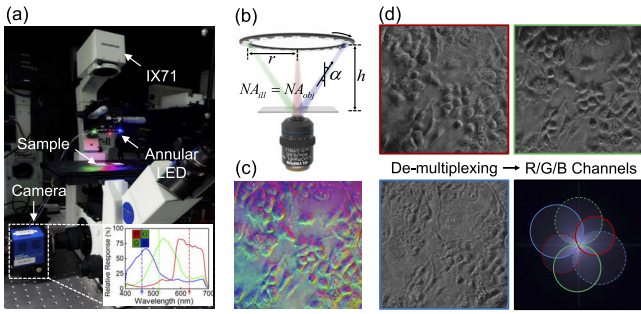
Fig. 2. Schematic diagram of color-multiplexed illumination in the sIDT imaging system. (a) Photo of the sIDT system, consisting of a standard inverted microscope, a programmable LED ring, and a color camera. (b) Three LEDs emit tri-color illumination from the LED ring to irradiate the sample simultaneously. The distance is tuned so that the illumination angle α is matched with the objective NA. (c) Captured color intensity image. (d) Three monochromatic intensity images corresponding to R/G/B channels separated from the color intensity image and the corresponding spectrum.
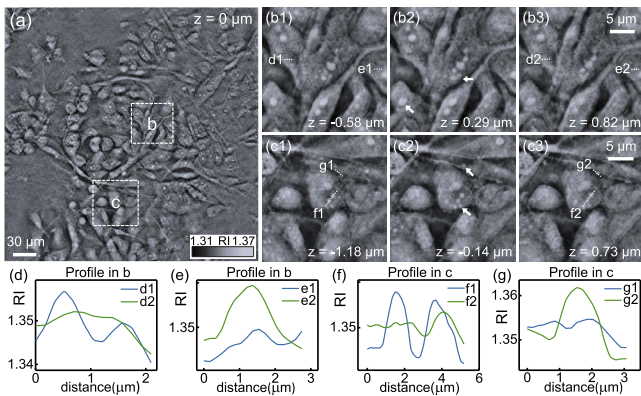
Fig. 3. Experimental 3D RI measurement of MCF-7 cells *in vitro*. (a) Large field of view image of MCF-7 cells reconstructed by the sIDT. (b),(c) Enlarged images of tomographic information at different depths of the two boxed regions in (a). (d)–(g) Comparison line profiles of intracellular structures on different depth slices.

Fig. 4. 3D RI reconstruction of a Spirulina algae specimen using sIDT. (a) Alternative color-multiplexed illumination pattern and its corresponding 3D Fourier spectrum. (b) 3D rendering results of the RI of the Spirulina using the three-frame sIDT algorithm. Additional 3D rendering view from different perspectives are shown in Visualization 1. (c) Four x–y direction slices of the RI distribution at different depths are recovered with one or three frames of sIDT. (d) Two RI slices along the x–z and y–z direction. (e1) and (e2) Corresponding line profiles of in (c) and (d).

of the objective (40×, 0.6 NA, LUCPLFLN, OLYMPUS), as illustrated in Fig. 2(b). Subsequently, the color camera records the scattered field of the specimen from different directions simultaneously as a color intensity image [shown in Fig. 2(c)]. Finally, three monochromatic intensity images corresponding to the R/G/B channels can be separated based on a color correction algorithm [shown in Fig. 2(d)] [21], and then used to recover the 3D RI distribution of the object.

We demonstrate the imaging performance of sIDT experimentally by measuring clusters of unstained MCF-7 cells distributed on a glass sample slide. Figure 3(a) shows the cells' RI distribution across $175 \times 175 \ \mu m^2$ at the objective's focal plane ($z = 0$). The RI slices of two zoomed areas in Fig. 3(a) are selected and highlighted as Figs. 3(b) and 3(c) to illustrate the subcellular structures inside MCF-7 cells. We can see the high-resolution features of cellular membrane folds, cell boundaries, and nuclei from the enlarged image. Meanwhile, we can see different intracellular features at different reconstruction depths [Figs. 3(b) and 3(c), white arrows]. As shown in Figs. 3(d)–3(g), the comparison line profiles of intracellular structures on different depths

slices [Figs. 3(b) and 3(c), white lines] illustrate that the sIDT method can realize 3D RI imaging.

It should be noted that the 4D TFs vary with wavelength since the radius of the pupil function $P(\mathbf{u})$ is inversely proportional to the illumination wavelength and the spectrum domain. Meanwhile, the frequency support region (i.e., Ewald spherical shells) in k-space can be obtained by Fourier transform of 4D TFs along the Z-axis in the presented sIDT method. Therefore, the tri-color illumination scheme in the sIDT results in the asymmetric coverage of Ewald spherical shells in 3D Fourier space, as shown in pattern 1 of Fig. 4(a) (three LED position interval 40°). Aiming at the near-isotropic 4D TFs, we further proposed an alternative illumination scheme. The illumination pattern 1 is rotated on the LED ring at an interval of 120° and obtained at t_n, t_{n+1}, and t_{n+2} moments (14 ms intervals) to form three illumination patterns that alternately illuminate the sample [Fig. 4(a)]. Then, the acquired three frames of color intensity images yield near-isotropic resolution and SNR at camera-limited frame rates to reconstruct complex RI.

To verify the accuracy improvement of sIDT, we experimentally measured a Spirulina algae specimen (3B Scientific, USA). Figure 4(b) displays the RI rendered as a 3D volume of Spirulina reconstructed with three illumination patterns. Figure 4(c) shows the x–y directions' slice information of different depths of Spirulina rebuilt in single and alternating illuminations. In addition, the x–z and y–z directions' slice information under alternating illuminations are shown in Fig. 4(d). In these results, we can clearly see the 3D spiral structure of Spirulina. Furthermore, when three illumination patterns are used in sIDT
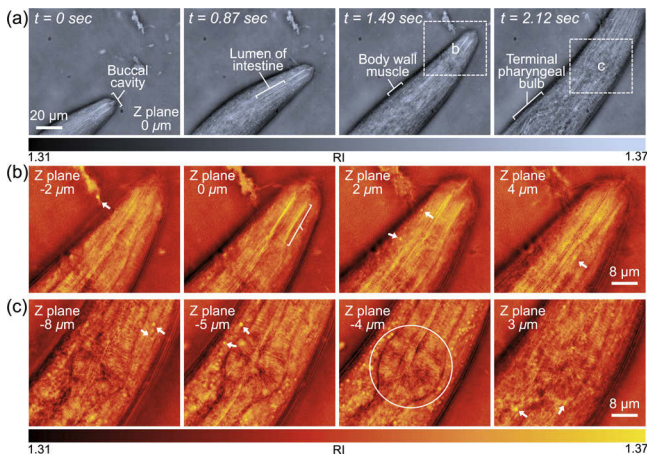
Fig. 5. Video-rate RI imaging of *C. elegans* using sIDT with three frames of color intensity images and an acquisition time of 14 ms per frame. (a) Recovered *C. elegans* position results at different moments during 2.12 s in Visualization 2. (b)–(c) Different depth information of the enlarged images of the two white boxes in (a).

technology, the internal structure of Spirulina becomes more precise and compact, as shown in Fig. 4(c). Meanwhile, the line profiles confirm that the more delicate structure of algae can be distinguished by using the three frames alternating illumination mode, as shown in Fig. 4(e1) [from 511 nm (lower line) to 437 nm (upper line)]. The experimental results demonstrate that sIDT can achieve near diffraction-limited lateral resolution of 437 nm and axial resolution of 2.58 μm.

Finally, we implemented the proposed sIDT method for the visualization and the quantitative analysis of the morphology of living samples (unstained living *Caenorhabditis elegans*). When measuring live samples, it is necessary to select appropriate frame rate and exposure time to reduce motion-related artifacts. Hence, the camera was optimized as a rectangular field of view consisting of 1920×1080 pixels to match the sample size and achieve the limit acquisition speed of 72 Hz in this experiment. In a time-lapse series, the reconstruction of each RI stack used three frames of color intensity images (covering 9 Ewald spherical shells). These images were acquired at an exposure interval of only 14 ms, allowing us to visualize 3D dynamic biological phenomenon with minimal motion artifacts and realizes real-time (~24 fps) imaging at the limited speed of the camera. Figure 5(a) shows the movement of the living *C. elegans* at the $z = 0$ μm plane for approximately 2 s in Visualization 2. The *C. elegans* at different time points in the imaging field and the parts of the *C. elegans* [Fig. 5(a), bracket] can be distinguished clearly. Figures 5(b) and 5(c) show the different depth information of the selected area of *C. elegans* at $t = 1.49$ s and 2.12 s in Fig. 5(a), respectively. Within the worm body, we recover the Lumen of intestine [Fig. 5(b), bracket] and the bulb [Fig. 5(c), circles] across multiple axial slices. Lipid droplets and lysosomes can also be distinguished at different axial layers [Figs. 5(b) and 5(c), arrows]. Experimental results demonstrate that sIDT is robust to motion artifacts and resolves internal features during high-speed worm motion.

In conclusion, we have proposed sIDT, a novel single-exposure tomographic technique based on color-multiplexed

illuminations enabling fast and high-resolution 3D RI imaging for unstained dynamic specimens. Compared with the existing monochromatic illumination-based IDT methods, we maximize the speed of 3D volumetric imaging through simultaneously chromatic illumination and compensate for the misalignment of 4D TFs both in the lateral and axial directions by self-calibration and cross correlation algorithms. Furthermore, the near-isotropic Fourier coverage along the transverse direction and real-time imaging capability are accomplished combining with the camera's maximum frame rates bandwidth limit and the three frames alternating illumination mode. The theoretical analysis and experimental results indicate that the sIDT is a promising 3D imaging technique for potential biomedical and life science applications.

REFERENCES

1. Y. Park, C. Depeursinge, and G. Popescu, Nat. Photonics **12**, 578 (2018).
2. G. Popescu, *Quantitative Phase Imaging of Cells and Tissues* (McGraw-Hill Education, 2011).
3. E. Wolf, Opt. Commun. **1**, 153 (1969).
4. Y. Sung, W. Choi, C. Fang-Yen, K. Badizadegan, R. R. Dasari, and M. S. Feld, Opt. Express **17**, 266 (2009).
5. R. Horstmeyer, J. Chung, X. Ou, G. Zheng, and C. Yang, Optica **3**, 827 (2016).
6. C. Zuo, J. Sun, J. Li, A. Asundi, and Q. Chen, Opt. Lasers Eng. **128**, 106003 (2020).
7. Y. He, B. Ge, M. Deng, Z. Yaqoob, G. Barbastathis, P. T. So, and R. Zhou, Proc. SPIE **11654**, 1165415 (2021).
8. A. Kuś, Opt. Lasers Eng. **149**, 106783 (2022).
9. J. M. Soto, Opt. Lett. **43**, 4699 (2018).
10. M. Chen, L. Tian, and L. Waller, Biomed. Opt. Express **7**, 3940 (2016).
11. J. Li, Q. Chen, J. Sun, J. Zhang, J. Ding, and C. Zuo, Biomed. Opt. Express **9**, 2526 (2018).
12. R. Ling, W. Tahir, H.-Y. Lin, H. Lee, and L. Tian, Biomed. Opt. Express **9**, 2130 (2018).
13. J. Li, A. C. Matlock, Y. Li, Q. Chen, C. Zuo, and L. Tian, Adv. Photonics **1**, 066004 (2019).
14. Z. F. Phillips, M. Chen, and L. Waller, PLoS One **12**, e0171228 (2017).
15. J. Sun, Q. Chen, J. Zhang, Y. Fan, and C. Zuo, Opt. Lett. **43**, 3365 (2018).
16. Y. Fan, J. Li, L. Lu, J. Sun, Y. Hu, J. Zhang, Z. Li, Q. Shen, B. Wang, R. Zhang, Q. Chen, and C. Zuo, PhotoniX **2**, 19 (2019).
17. A. Matlock and L. Tian, Biomed. Opt. Express **10**, 6432 (2019).
18. X. Ou, R. Horstmeyer, G. Zheng, and C. Yang, Opt. Express **23**, 3472 (2015).
19. M. Guizar-Sicairos, S. T. Thurman, and J. R. Fienup, Opt. Lett. **33**, 156 (2008).
20. J. Li, A. Matlock, Y. Li, Q. Chen, L. Tian, and C. Zuo, Photonics Res. **8**, 1818 (2020).
21. Y. Wu, Y. Zhang, W. Luo, and A. Ozcan, Sci. Rep. **6**, 28601 (2016).